Plasma Phys. Control. Fusion 37 (1995) 1015–1030. Printed in the UK

Dynamic plasma behaviour excited by $m = \pm 1$ helicon wave

Shunjiro Shinohara, Yoko Miyauchi and Yoshinobu Kawai

Interdisciplinary Graduate School of Engineering Sciences, Kyushu University, Kasuga, Fukuoka 816, Japan

Received 20 March 1995, in final form 15 May 1995

Abstract. The dynamic behaviour of a plasma produced by a helicon wave using exciting $m = 1$ and -1 helical modes is investigated. The RF (radio frequency) power dependence, antenna–plasma coupling, and time evolution of plasma parameters and Ar line intensities are studied in relation to the density jump, i.e. a steep increase in density to a level of 10^{13} cm^{-3} by the application of an RF input power greater than 1 kW. Before the density jump, the excited wave is localized near the antenna, exhibiting a standing wave character. After the jump, this wave propagates outwards and a dispersion relation for the helicon wave is confirmed.

1. Introduction

The production of a high-density plasma using a helicon wave [1–6] as a high-density plasma source has become very attractive in confinement devices as well as in plasma processing ones. It has been shown that a high-density plasma of up to $\geqslant 10^{13}$ cm^3 could be produced efficiently by the application of RF (radio frequency) waves to the axial magnetic field B_0 of more than several hundreds of G. In addition, a helicon wave, satisfying a dispersion relation [3, 6] and expected magnetic field distributions [1, 4, 6], was observed with a decreasing spatial amplitude.

However, it should be stressed that the essential role in plasma production including plasma initiation solely by a helicon wave has not been verified up to the present. In relation to this, we have not clarified the 'density jump' phenomenon, which is characterized by a steep (abrupt) increase in the plasma density to a level of 10^{13} cm^{-3} with more than a threshold RF power P_{th} of $\leqslant 1$ kW within a time scale of several hundreds of μs.

Moreover the behaviour over time (especially from plasma initiation to the established phases) and the space structures of the plasma parameters including excited wave fields have scarcely been studied, in spite of the active and intensive use of this wave as a plasma production tool, e.g., in the plasma processing field. Needless to say, even the basic database of plasma parameters is inadequate. The findings obtained so far are incomplete and the mechanism and behaviour of production and sustainment are still open questions to be studied.

To study this mechanism, we investigate the dynamic behaviour of a helicon-wave-produced plasma in detail and systematically. Here in this paper, after describing an experimental system in section 2, the spatiotemporal plasma parameters (in section 3) and their dependences on RF power (in section 4) are presented: the electron temperature, electron density and ion saturation current, including the antenna plasma resistance (antenna–plasma coupling) as well as Ar I and Ar II line intensities, are measured. In section 5, the

0741-3335/95/091015+16$19.50

history of the wave on the (ω_p, $k_\parallel$) plane (ω_p is the angular frequency of the plasma, $k_\parallel$ the parallel wavenumber) both inside and outside the antenna regions, in addition to the wave patterns, is investigated for the first time to analyse the nature of the excited wave. Finally, conclusions are presented in section 6.

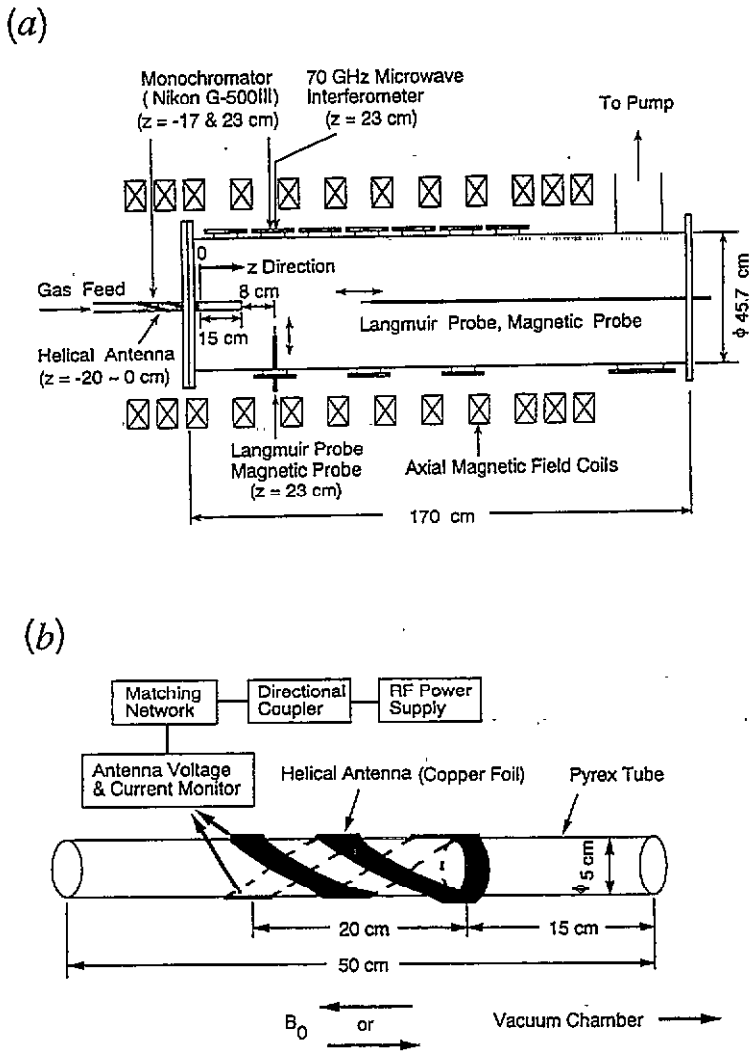

Figure 1. Schematic views of (*a*) the experimental apparatus and (*b*) the antenna structure including RF system.

2. Experimental set-up

The experimental system is shown in figure 1. The filling pressure of the Ar gas, fed into the left-hand side of the Pyrex tube (the inner diameter is 5 cm and total length is 50 cm, the axial position of $z = -35 \sim 15$ cm), is 0.6 mTorr with a static axial magnetic field of $B_0 = 1$ kG typically. Here, $z = 0$ cm is defined at the right-hand side of a helical antenna.

The RF power and frequency are less than 3 kW and 7 MHz, respectively, and a RF pulse width is 2 ms with a duty of < 0.1 (pulse repetition rate < 50 Hz) to prevent thermal damage to the helical antenna and RF system. The RF power supply is connected to the antenna through a directional coupler, which picks up the incident and reflected power, i.e. P_{inc} and P_{ref}, a matching box (split tank circuit) and monitors for the antenna's voltage and current. The antenna length is 20 cm ($z = -20 \sim 0$ cm) with a one-turn winding, made of copper foil 2.5 cm wide and 0.25 cm thick, around a Pyrex tube. The exciting $m = 1$ or -1 modes (m is the azimuthal mode number) can be selected by changing the sign of the axial magnetic field B_0 in this system. Here, $m = 1$ (-1) denotes right-hand (left-hand) rotation with respect to the magnetic field B_0.

The plasma parameters and excited wave fields are measured by movable Langmuir and magnetic probes inserted into the plasma, respectively. A balanced mixer for the interferometric wave measurements and a boxcar integrator for averaging the obtained data are also used. A 70 GHz microwave interferometer for measurement of the absolute plasma density and a visible monochromator (focal length 50 cm) are also installed.

3. Spatiotemporal plasma behaviour

The time evolution of n_e (electron density), T_e (electron temperature), Ar I (419.8 nm) and Ar II (488.0 nm) line intensities are shown in figure 2 ($m = 1$, $P_{inp} = 1.4$ kW (hereafter P_{inp} is defined at $t = 1.8$ ms unless otherwise stated)) and figure 3 ($m = -1$, $P_{inp} = 1.2$ kW). Here, the RF input power P_{inp} is $P_{inc} - P_{ref}$ and the net power P_{net} is defined as $(P_{inc} - P_{ref}) \times R_p/(R_v + R_p)$, where $R_v (= 0.27\ \Omega)$ and R_p are the vacuum and plasma loading resistances, respectively (antenna–plasma coupling will be described in section 4). Note that the power reflection coefficient $R = P_{ref}/P_{inc}$ is typically less than 0.3 at $t > 0.5$ ms.

These parameters are measured outside ($z = 23$ cm by a Langmuir probe and a monochromator) as well as inside ($z = -17$ cm by a monochromator) the antenna regions. The electron density n_e measured by Langmuir probes is carefully calibrated by a 70 GHz microwave interferometer, which is important in determining the absolute value (e.g. the influx on the substrate to aid plasma manufacture and a dispersion relation depending on the plasma density), but it has not been used much up to now.

The electron density n_e is low for about 0.2 ms after that application of RF power, but this density increases suddenly to a level greater than 10^{13} cm^{-3} (the so called 'density jump') after that. When P_{inp} is lower than a threshold value P_{th} of about 1 kW, n_e, Ar I and Ar II line intensities remain low during the whole 2 ms RF pulse (the dependences of the plasma parameters on P_{inp} are shown in figures 8 and 9). After the density jump with a decrease in the electron temperature, the Ar II (Ar I) intensity increases (decreases), which shows a neutral density decrease and a higher ionization rate.

These phenomena are more pronounced for the $m = -1$ case, and the behaviour of the Ar line intensities over time is similar to the $B_0 = 0.5$ kG case. Note that Ar I (Ar II) intensity may be proportional to $n_e n_0 \langle \sigma v \rangle_I (n_e n_i \langle \sigma v \rangle_{II})$, where n_0, n_i, σ and v are the neutral density, ion density, cross section and electron velocity, respectively, and $\langle \sigma v \rangle_I$ and $\langle \sigma v \rangle_{II}$ are functions of the electron temperature, assuming a Maxwellian electron velocity distribution.

For the $m = 1$ excitation case, the relative Ar I and Ar II line intensities in the outside region, which are normalized by the respective intensities in the inside region, are higher than those for $m = -1$ excitation due to the different axial plasma density profile: the effective plasma length along the z axis is longer for the $m = 1$ case as shown in figure 7.

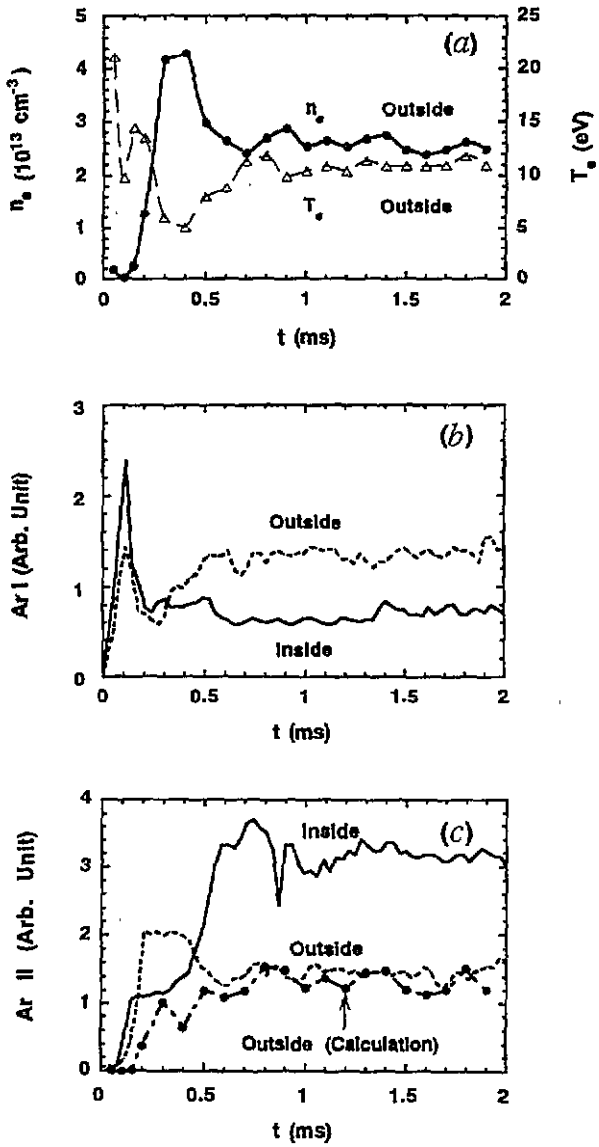

Figure 2. Time evolution of (*a*) electron density n_e and electron temperature T_e, (*b*) Ar I (419.8 nm) and (*c*) Ar II (488.0 nm) line intensities for $m = 1$ excitation.

There is a tendency for the electron temperature T_e in the outside region to be higher for $m = 1$ excitation than for $m = -1$ excitation (see figures 2(*a*), 3(*a*) and 8(*b*)), and the n_e in the antenna region for $m = -1$ excitation is higher than that in the outside region (not shown), which is consistent with the result in figure 7(*b*).

The evolution of the Ar II line intensity can well be simulated after the establishment of the plasma, as shown in figures 2(*c*) and 3(*c*). This intensity, which is proportional to $n_e n_i \langle \sigma v \rangle_{II}$, is estimated by the use of the experimental values of $n_e (= n_i)$ and T_e, based on the cross section data dependent on T_e [7]. There is a controversy whether high-energy electrons (several tens of eV) exist or not [8]. With an increase in the electron temperature from a few eV to several tens of eV, the Ar II line intensity increases dramatically by more than two orders of magnitude, according to the calculation using the cross section data [7]. From this, the experimental results in figures 2(*c*) and 3(*c*) suggest that even if exists,

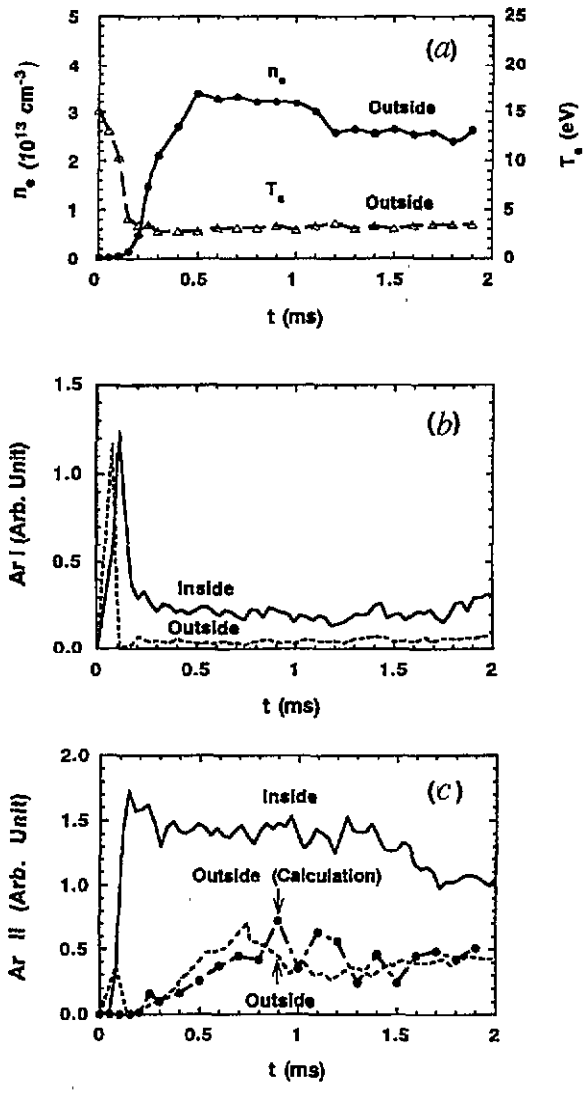

Figure 3. Time evolution of (*a*) electron density n_e and electron temperature T_e, (*b*) Ar I (419.8 nm) and (*c*) Ar II (488.0 nm) line intensities for $m = -1$ excitation.

there is a small portion of high electron energy component (more than 10 eV). In contrast, the number of high-energy electrons may be somewhat larger during the plasma formation phase, since a small hump in this Ar II intensity can be seen.

Figure 4 shows changes in the ion saturation (radial) current profiles I_{is} in the outside region ($z = 23$ cm) with time for (*a*) $m = 1 (P_{inp} = 2.2$ kW) and (*b*) $m = -1 (P_{inp} = 1.6$ kW) excitation. As can be seen, I_{is} is small and broad before the density jump. After the jump I_{is} abruptly becomes large but this profile for the $m = -1$ case is more peaked than for the $m = 1$ case. This can also be found from the n_e measurements ($z = 23$ cm) in figures 5(*a*) ($P_{inp} = 1.7$ kW, $m = 1$) and 6(*a*) ($P_{inp} = 1.4$ kW, $m = -1$).

The more peaked profile for the $m = -1$ case may reflect the fact that the effect of the heating profile is stronger than the diffusion effect; the radial profile of the energy dissipation term of $\langle E_z * j_z \rangle$ (product of the z-component of the excited electric field by that of current) due to the collisional damping is expected to be more peaked for the $m = -1$ case [4, 5],

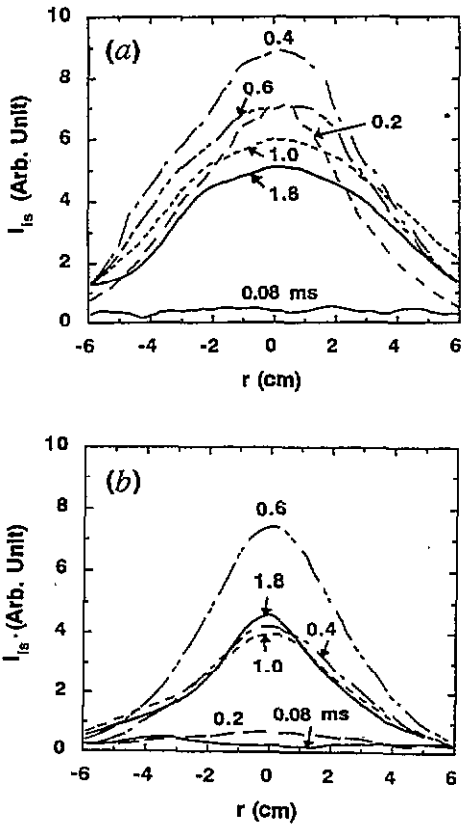

Figure 4. Time evolution of radial profiles of ion saturation current for I_{is} for (*a*) $m = 1$ and (*b*) $m = -1$ excitation at $z = 23$ cm.

i.e. near the peak of the z-component of the excited magnetic field B_z. Therefore, a narrow dense profile for $m = -1$ excitation and a broad, uniform profile for $m = 1$ can be expected according to [5]. In contrast, the wave-induced radial transport is worse for the $m = -1$ case than that for $m = 1$ case [9], but this has not been discussed very much quantitatively.

Here, the global energy confinement time is several tens of μs in our experimental conditions. Although experimental diffusion has not been explained quantitatively up to now in the straight magnetic field configuration, the axial energy confinement time (ambipolar diffusion) is estimated to be greater than 100 μs, which is smaller than the radial one by a factor of few times (minor radius is comparatively small). Note that the parallel (along the magnetic field line) transit time through the plasma by the ion sound speed is $\geqslant 100$ μs.

Therefore, even though the radial diffusion due to the excited wave is altered by the sign of m, this contribution may be smaller than the heating profile effect. Needless to say, the effects of anomalous diffusion and another azimuthal mode, such as $m = 0$ or a higher radial mode (see equation (35) in [2]), must also be taken into account to interpret the obtained profile quantitatively. As the density profile is also governed by the neutral density near the outer plasma region, further studies (such as confinement and excited wave field measurements) are needed to understand this difference in profile.

Figures 5(*a*) and 6(*a*) show that the electron temperature T_e is nearly constant (it gradually decreases with the plasma radius) and higher (lower) for the $m = 1$ ($m = -1$) case. In figures 5(*b*) and 6(*b*), the electron pressure $P_e = n_e k T_e$ (k is the Boltzmann constant) is also more peaked for the $m = -1$ case (see figures 4, 5(*a*) and 6(*a*)) with a lower space potential V_{sp} compared with the $m = 1$ case.

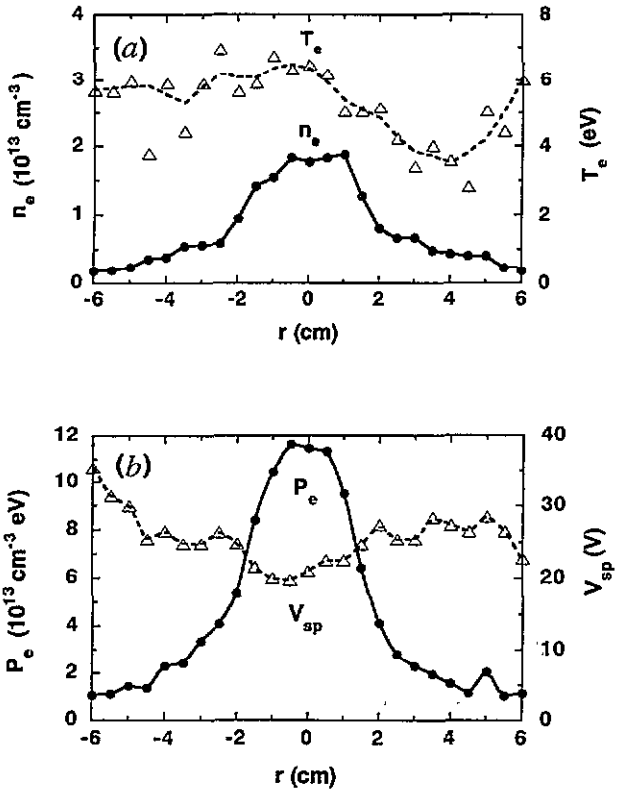

Figure 5. Radial profiles of (*a*) electron temperature T_e and density n_e, and (*b*) electron pressure $P_e \equiv n_e k T_e$ and space potential V_{sp} for $m = 1$ excitation at $z = 23$ cm.

Figure 7 shows the time evolution of the axial profiles of the ion saturation current I_{is} for (*a*) $m = 1$ ($P_{inp} = 1.1$ kW) and (*b*) $m = -1$ ($P_{inp} = 1.2$ kW) excitation, measured at the plasma centre of $r = 0$ cm. At an early stage after the density jump for the $m = 1$ case, I_{is} is peaked near the antenna region, then the peak position moves outwards (positive z direction) with time. Previous results with lower RF power shows that n_e and $I_{is}(T_e)$ increase (decreases) with z position ($z < 50$ cm) at a later stage in the establishment of the plasma with almost constant electron pressure P_e along the z axis. For higher RF power, I_{is} and P_e gradually decrease with the z position ($20 < z < 60$ cm region).

For the $m = -1$ case, in contrast, the I_{is} peak is localized near the antenna region and I_{is} decreases with an increase in the positive z position (a slight change in profile with time). This localization of I_{is} may come from larger collisional damping due to the higher plasma density near the antenna.

4. Power dependence

In this section, the relationship between the plasma parameters and input power P_{inp} is presented. Figure 8 shows the dependences of n_e and T_e, outside ($z = 23$ cm) the antenna region of $r = 0$ cm, on input RF power P_{inp} for the $m = 1$ and -1 excitation. When P_{inp} is greater than a threshold power P_{th} of about 1 kW, an electron density jump of three orders of magnitude (from the order of 10^{10} to that of 10^{13} cm^{-3}) with a drop in

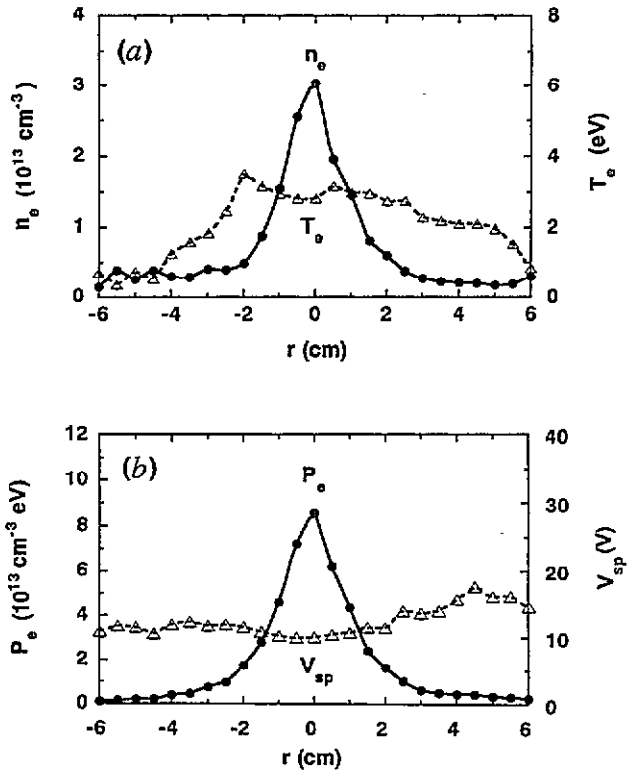

Figure 6. Radial profiles of (a) electron temperature T_e and density n_e, and (b) electron pressure $P_e \equiv n_e k T_e$ and space potential V_{sp} for $m = -1$ excitation at $z = 23$ cm.

the electron temperature (from 10–15 to 3–8 eV) is found, i.e. a clear discontinuity in the electron density at P_{inp} is found near P_{th} (see the bold arrow with impedance matching in figure 8(a)). There is no appreciable difference between the P_{th} for the $m = 1$ and -1 excitation for this density jump.

In the high-density region (after the jump), n_e changes little even though P_{inp} is further increased, which implies saturation of the ionization, i.e. nearly complete ionization for the fixed filling pressure (the same saturation trend is found in figure 9 for the Ar II line intensity). In this high-density region, T_e in the outside region ($m = 1$) and n_e in the inside region ($m = -1$) are higher than other cases by a factor of less than 3.

In this experiment as stated before, the power reflection coefficient $R = P_{ref}/P_{inc}$ is typically less than 0.3 at $t > 0.5$ ms for both high and low plasma densities by adjusting the capacitance values in the matching box. Needless to say, R is high in the initial stage (before the density jump) of the RF pulse for the high power case of $P_{inp} > P_{th}$, although R is low after the density jump at the later stage. If we keep capacitance values in the matching box constant and increase the RF power from a low value (R is also low), n_e increases dramatically near $P_{inp} = P_{th}$ but P_{inp} suddenly becomes low due to mismatch (a large reflection of $R > 0.5$); the trajectory is depicted in figure 8(a) (see a double-line arrow without impedance matching and crosses for the large R case ($m = 1$)). Here a P_{inp} of both about 1 kW (just before the density jump) and about 0.5 kW (the lowest data of crosses in figure 8 after the jump) correspond to $P_{net} = P_{inp} \times R_p/(R_v + R_p)$ of about 0.4 kW.

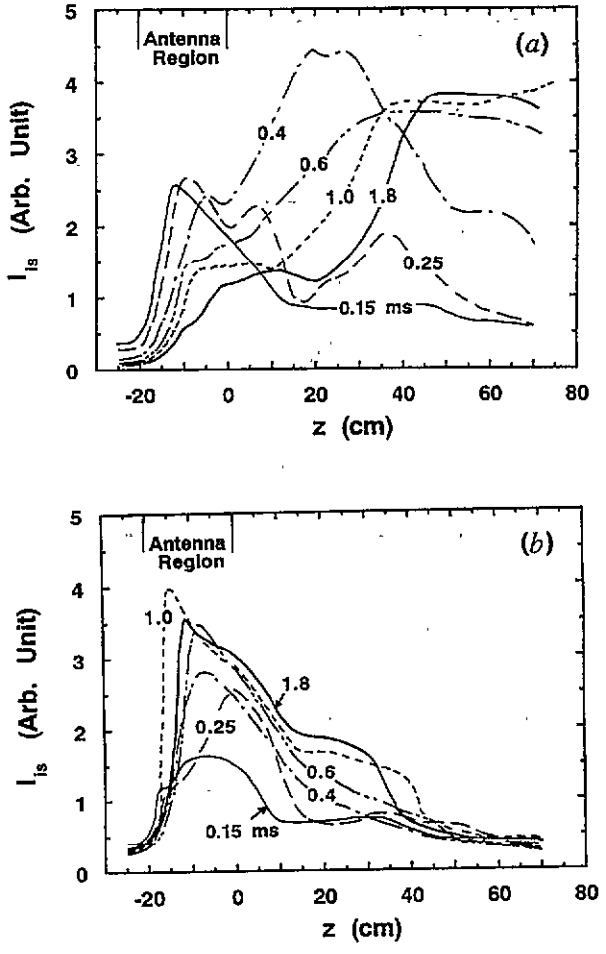

Figure 7. Time evolution of axial profiles of ion saturation current I_{is} for (*a*) $m = 1$ and (*b*) $m = -1$ excitation at $r = 0$ cm.

For this large reflection case, only $P_{inp} > 0.5$ kW is necessary to give high-density plasma but distorted electric fields exist due to this large R. This suggests that a high electric field, especially the near-field (inductive field), is also important in obtaining a high-density plasma as well as generating the initial plasma.

Antenna–plasma coupling is studied by changing the RF power P_{inp}. Before a density jump of $P_{inp} < P_{th}$, the plasma loading resistance R_p is low, i.e. about 0.2 Ω ($\leqslant$ the vacuum loading of R_v). This R_p increases dramatically after the density jump, and then remains nearly constant with P_{inp} (the same feature is obtained with the relationship between n_e and P_{inp} in figure 8(*a*)). For the high-density region, a good coupling efficiency $\eta = R_p/(R_v+R_p)$ of about 0.9 is obtained, which means a lowering in the RF applied voltage on the antenna (desirable for reducing the direct acceleration of the charged particles near the antenna, which is critically important for the material processing). The total inductance of the antenna including the feeder part during the experiments is about 0.4 μH, which differs little between cases with and without plasma (and also regardless of the plasma density).

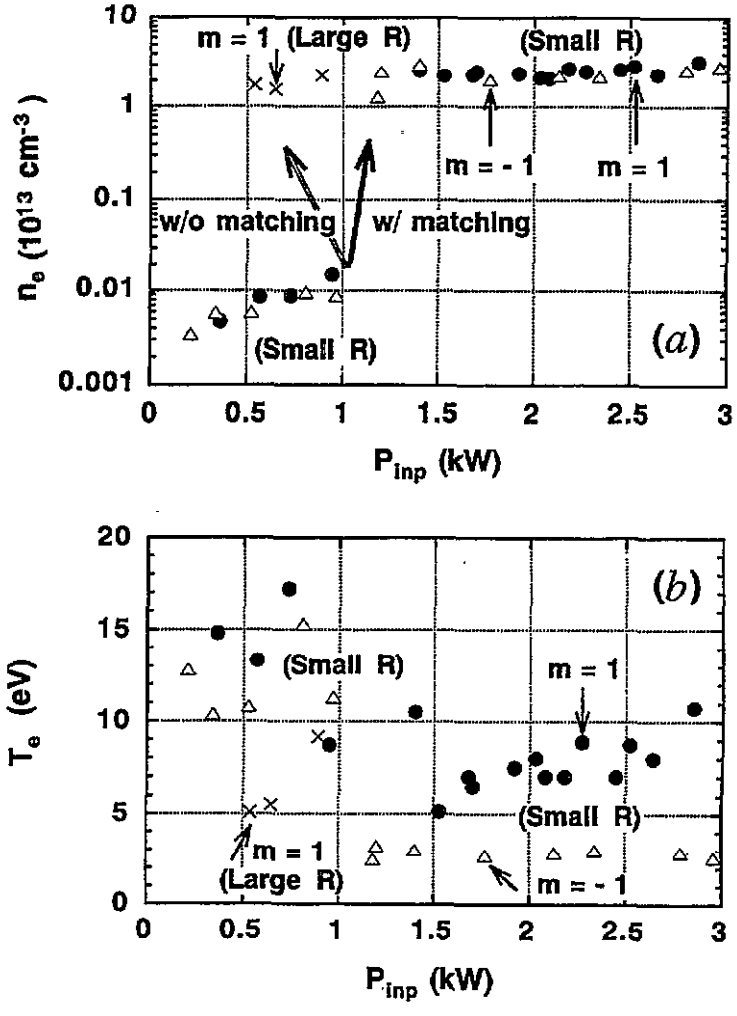

Figure 8. Dependences of (*a*) electron density n_e and (*b*) electron temperature T_e on input RF power P_{inp} for $m = 1$ and -1 excitation at $z = 23$ cm. Here, full circles, open triangles and crosses represent excitation of $m = 1$, $m = -1$ and $m = 1$ with a large reflection $R = P_{ref}/P_{inc}$, respectively. A bold arrow shows the trajectory with unchanged low R by adjusting matching circuit values (with impedance matching), and a double-line arrow shows that from small R to large R without a change in circuit values (without impedance matching), near the density jump region.

Next, the plasma loading resistance R_p is studied as a function of the plasma density n_e near the antenna position ($r = 0$ cm and $z = -5$ cm), because R_p is considered to depend mainly on the local plasma density facing the antenna. As R_p and n_e behave similarly with P_{inp} mentioned above, R_p is low (about 0.2 Ω) before the density jump ($P_{inp} < P_{th}$) and becomes higher (1–2 Ω) by nearly one order of magnitude after that ($P_{inp} > P_{th}$). In regions of both low and high density, R_p is weakly dependent on n_e and there is a slight difference in the dependence between the $m = 1$ and -1 cases.

This value of R_p obtained after the density jump shows a comparative or somewhat stronger plasma coupling normalized by the antenna size length and width, compared with

a fast magnetosonic wave [10, 11] and an ion Bernstein wave [11, 12] in the ion cyclotron range of frequency (ICRF) in the small tokamak TNT-A. Comparing the experimental plasma conditions, the central electron temperature (density) for the present case is lower (higher) than that of those waves by one order of magnitude (a few times). This leads to a collision frequency which is higher by two orders of magnitude with the plasma cross section being smaller by one order of magnitude (than the previous ICRF experiments in the TNT-A machine).

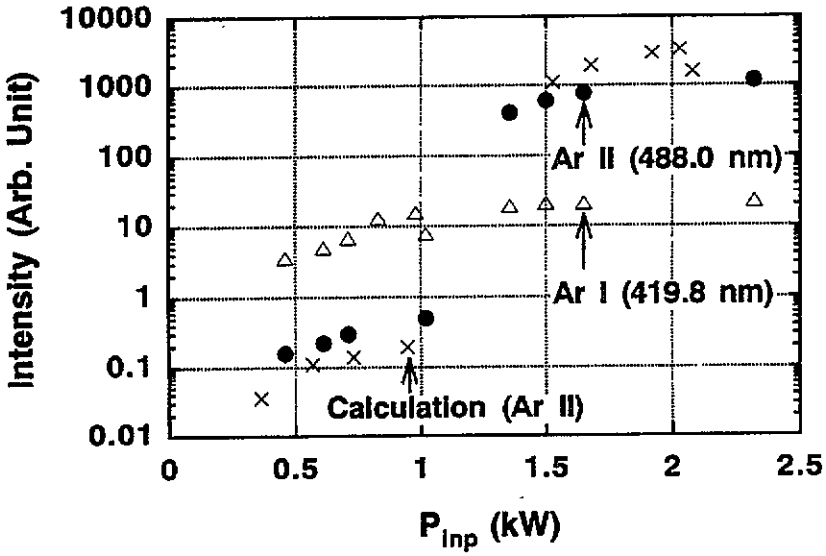

Figure 9. Ar I (419.8 nm) and Ar II (488.0 nm) line intensities against P_{net} for $m = 1$ excitation at $z = 23$ cm. Here, open triangles, full circles and crosses represent experimental line intensities of Ar I, Ar II and calculation line intensity of Ar II, respectively.

The dependence of the Ar I (419.8 nm) and Ar II (488.0 nm) line intensities on the input power P_{inp} are shown in figure 9 for $m = 1$ and excitation at the outside ($z = 23$ cm) antenna region. After the density jump, the Ar II intensity increases by more than two orders of magnitude, whereas the Ar I intensity only increases slightly (similar results are obtained for the $m = -1$ excitation case). When the large reflection ($R > 0.5$) data after the density jump are added, a similar trajectory (like the double-line arrow in figure 8(a)) can also be obtained. The dependence of the Ar II intensity on P_{inp} is also consistent with the calculation (the same procedure described in section 3).

5. Time evolution of wave structures

The history of the excited wave feature is studied on the $(\omega_p, k_\parallel)$ plane to check the dispersion relation, as shown in figures 10(a) ($m = 1$) and (b) ($m = -1$) with $P_{inp} = 1.9$ kW. Here, the $k_\parallel$ value, averaged over 0.5–1 wavelength along the z axis ($r = 0$ cm), is determined by the magnetic probe signal using the interferometric method with the antenna current. Here, the antenna's excited fundamental $k_\parallel$ value in the vacuum $k_{\parallel a}$ is 0.31 cm^{-1}. The plasma density n_e used to calculate ω_p is measured at $z = -5$ cm (inside) and 23 cm (outside), and $\omega_p = 1.8 \times 10^{11}$ rad s^{-1} corresponds to $n_e = 10^{13}$ cm^{-3}.

In this figure, two calculation curves for a (plasma radius) = 2.5 cm and 4 cm cases are

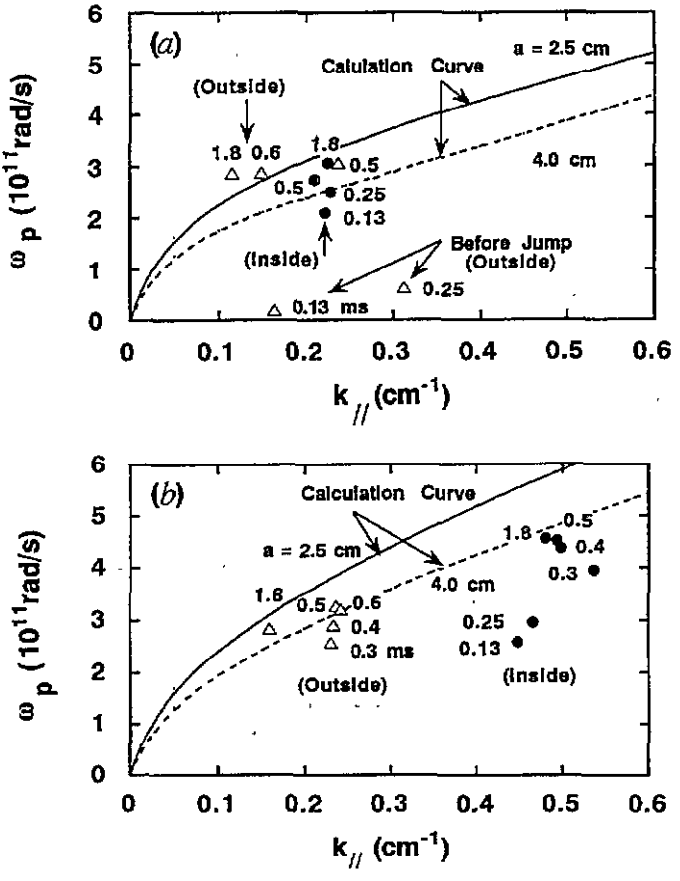

Figure 10. History of the dispersion relation on (plasma frequency, parallel wavenumber) = (ω_p, $k_\parallel$), plane for (*a*) $m = 1$ and (*b*) $m = -1$ excitation at $r = 0$ cm. Here, full circles and open triangles show the cases measured inside and outside the antenna regions, respectively.

drawn, taking the first radial mode in equation (35) [2]. Experimentally a is about 2.5 cm inside the antenna region and $\geqslant 2.5$ cm outside it: the effective plasma radii at the outside region are about 3 cm for $m = 1$ excitation and 2.5 cm for $m = -1$ (see figures 5(*a*) and 6(*a*)), neglecting slopes at the larger radii.

Before the density jump, a wave does not very often propagate to the outer side of the antenna region (see figure 11(*a*)). The dispersion relation of the helicon wave, whose wave is a whistler wave with boundary conditions [2], is not satisfied at the outside region (see $t = 0.13$ and 0.25 ms in figure 10(*a*)). This can also be confirmed from figure 11(*a*) before the density jump: $k_\parallel = 0.3$ cm^{-1} (nearly the same value with the fundamental antenna excited wavenumber $k_{\parallel a}$) with a low ω_p value. In addition, a preliminary measurement of the excited magnetic fields at $z = 23$ cm shows different radial profiles before and after the density jump.

Considering the present experimental conditions, only the whistler wave can propagate into the plasma. This wave, i.e. the R (right-hand circular polarization) wave, can be expressed approximately as $k_\parallel^2 = \omega\omega_p^2 \cos\theta/\omega_{ce}c^2$ (ω is the excited RF angular frequency, ω_{ce} the electron cyclotron angular frequency, c the light velocity, θ the propagation angle with respect to the axial magnetic field) without imposing boundary conditions. Even though

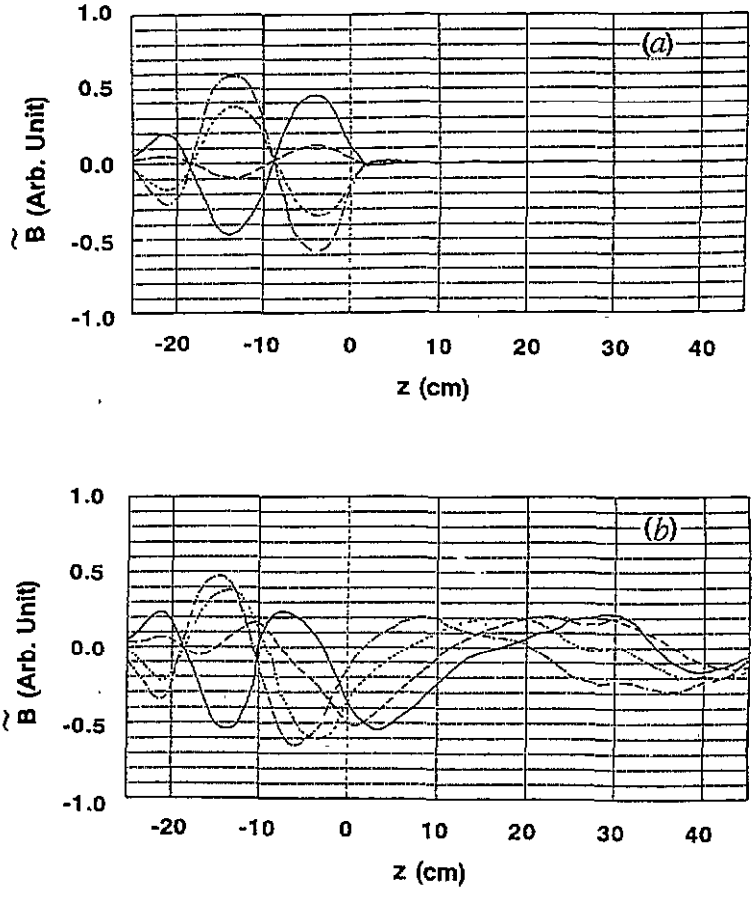

Figure 11. Typical wave patterns of excited perpendicular magnetic field at (*a*) $t = 0.03$ ms and (*b*) $t = 1.8$ ms for $m = 1$ excitation at $r = 0$ cm. Here, full, broken, dotted and chain lines represent cases of phase $\Delta\phi = 0$, -0.21π, -0.45π and -0.66π, respectively.

we take $\theta = 0°$ (parallel direction), the dispersion relation for the R wave at $t = 0.13$ ms and 0.25 ms is not satisfied: the experimental ω_p value is smaller by a factor of several times.

After the jump shown in figure 10, this relation holds good for both inside and outside the antenna region. For the $m = -1$ case, the $k_\parallel$ value in the inside region is higher than that in the outside one, and the ω_p value is somewhat smaller at the early phase after the density jump (for reference the $k_\parallel$ value at $t = 0.13$ ms is nearly the same value expected from the R wave with $\theta < 10°$, discussed above). The time taken to satisfy this dispersion relation of the helicon wave is shorter inside the antenna region than outside, because of the faster rise in density in the inside region. Note that the observed wavenumber after the jump is not decided by the antenna ($k_{\parallel a}$) but by the plasma, i.e. the dispersion relation. These features before and after the density jump are also confirmed for the $B_0 = 0.5$ kG case.

Now, we discuss the errors in the experiment and calculation, because these errors are important for a quantitative agreement between theoretical and experimental results. As for the experiments, the error in the plasma density in total is less than 20%, which means less

than 10% relative error in estimating the value of ω_p. This n_e error comes from a calibration of the absolute value, a reproducibility and plasma perturbation by the Langmuir probe, i.e. n_e becomes somewhat lower ($< 15\%$) for the deep probe insertion case. The error in the $k_\parallel$ value due to the averaging, reproducibility and perturbation, measured by magnetic probes, is also considered to be less than 20%.

In the calculation, the increase in the ω_p value for the fixed $k_\parallel$ value is estimated to be less than 15% if we take another azimuthal mode number such as $m = 0$ mode in place of the $m = 1$ or -1 modes. Preliminary wave measurement indicates that the normalized $m = 0$ mode amplitude is less than 20% after the plasma has been established, which means less than 3% error in the ω_p estimation. The effect of the second radial mode is also considered to be small. Although a wall radius effect is negligible ($< 10\%$) [4], a density profile effect for the $m = -1$ case is large (the profile effect is negligible for the $m = 1$ case). According to a calculation from [4] and [5], a peaking of the density profile from the uniform to parabolic profiles lowers the ω_p value by less than twice that for the same $k_\parallel$ value, which shows that the expected calculation curves in figure 11(b) become closer to the experimental values. Therefore, the above mentioned conclusions need not be altered as a result of this discussion.

Figure 11 shows typical wave patterns along the z axis for $m = 1$ excitation before the density jump at $t = 0.03$ ms and after that at $t = 1.8$ ms ($P_{inp} = 1.2$ kW). Here the perpendicular components of the excited magnetic field at the plasma centre ($r = 0$ cm) are measured by the interferometric method with the use of the boxcar integrator (full width of the time window is less than 0.04 ms). The various curves represent the different phases $\Delta\phi$ between the excited wave and antenna current in one RF cycle of 7 MHz by use of a phase shifter.

Before the jump, the excited wave is localized at the antenna region with a standing wave character: nodes and loops can be clearly seen regardless of the phase. After the jump, we can interpret that this wave propagates outwards to the right (positive z direction), considering the phase $\Delta\phi$ and wave patterns at the positive z position in figure 11(b). In contrast, a standing wave still exists in the inside antenna region (especially in the left region). The increase in the plasma boundary with time (see figure 7(a)) increases the amplitude of the magnetic field with the wider excited region moving to the right. Nearly the same features are obtained for $m = -1$ excitation as well as by the signal of the excited parallel magnetic field component. However, the excited wave is more localized near the antenna (it only exists at $z < 20$ cm with a smaller amplitude) for $m = -1$ excitation than for $m = 1$ excitation after the density jump, since there may be larger collisional damping due to the higher plasma density near the antenna (see figure 7).

Here, we consider the nature of the wave appearing in this experiment (figure 11). In the antenna region before the density jump (low plasma density), a wave, which does not satisfy the dispersion relation of the helicon wave, can be forced to have a wavenumber of $k_{\parallel a}$ (antenna excited wavenumber) with a boundary near the left- and right-hand sides of the antenna: a standing wave can exist as shown in figure 11(a).

When the excited wave satisfies this dispersion relation after the density jump near the antenna region (not at the outside region), a wave with the $m = 1$ mode can propagate to the right and the $m = -1$ mode to the left, although the directivity may be not so good since the antenna length is comparable with the excited wavelength. If there is a boundary (this boundary may be determined by the plasma region) near the antenna and the amplitudes of both modes are the same, a standing wave can also exist (there may be a wall($z = -35$ cm)-reflecting effect at the left-hand side of the antenna region). After the density jump, in the outside region, the plasma boundary also moves to the right, and

the excited wave can propagate to the right with a standing wave character partly near the antenna region (figure 11(*b*)).

We can rule out the possibility that, after the jump, this wave which can be thought of as a standing wave near the antenna discussed above, is composed of fundamental and higher harmonics (integer n) wavenumbers with the same amplitudes; if there is a harmonic component, the obtained $k_\parallel$ value changes in appearance by a factor of $(n-1)/2$. Therefore, the excited wave does not satisfy the expected dispersion relation for the helicon wave shown in figure 10, as the real experimental $k_\parallel$ values change by a factor of $2/(n-1)$ (fundamental component) and $2n/(n-1)$ (harmonic component). In addition, it is difficult to excite the fundamental and higher harmonics components only, omitting the counter propagating wave, and also difficult to explain the wave patterns in outside antenna regions on the left- and right-hand sides.

Finally, we discuss a mechanism for high-density plasma production (a sudden density jump) briefly from the experimental results. Before the density jump, the near-field effect (especially the inductive field near the antenna) is important to have a low density plasma of order of 10^{11} cm^3 and relatively higher electron temperature (figure 8): a plasma and excited wave fields, which do not satisfy the dispersion relation (figure 10), are localized near the antenna (figures 7 and 11(*a*)). Here, the capacitive coupling effect seems to be small due to the slight change in the antenna inductance stated before. In contrast, for the ICP (inductively coupled plasma) case with higher filling pressure and without the axial magnetic field, capacitive coupling may exist before the density jump [13]. Before this jump in our experiment, the plasma density n_e increases almost linearly with an increase in the input power P_{inp}, while the electron temperature T_e remains higher (10–15 eV range) than that after the jump.

When the power P_{inp} (in other words, electric field) exceeds a threshold value of about 1 kW, the plasma density n_e increases dramatically like an avalanche (figure 8) due to a cooperation effect as the increase in n_e accelerates the plasma loading resistance R_p, which leads to an increase in the net absorbed power P_{net} by the plasma. When the density becomes higher, the excited wave (figure 10) can propagate as a helicon wave from the antenna to the outer regions (figure 11(*b*)) and the high-density plasma is produced by collisional and electron Landau damping (collisional damping is stronger than electron Landau damping from calculation, and experimental damping length is discussed in [3]). However, detailed spatiotemporal measurements of plasma parameters and wave excited fields including the electric fields will be necessary to draw a definite conclusion to explain the observed phenomena.

6. Conclusions

The dynamic behaviour of a plasma produced by a helicon wave using exciting $m = 1$ and -1 helical modes is investigated. When the input RF power P_{inp} is greater than about 1 kW (net RF power $P_{net} > 0.4$ kW), a density jump with dramatic increases in the plasma loading resistance R_p and Ar II line intensity are observed. After this jump, the electron temperature T_e and Ar I line intensity become lower, whereas the Ar II line intensity increases. The RF power dependence and time evolution of the Ar II line intensity experimentally obtained are consistent with the calculation results.

The time evolution of radial and axial profiles such as I_{is} (ion saturation current) shows different features between $m = 1$ and -1 excitation; for $m = -1$ excitation, I_{is} is localized near the antenna (along the z axis) and a peaked radial profile (n_e is also peaked) is observed. In contrast, the peak position of I_{is} moves axially outwards with time for $m = 1$ excitation.

Before the density jump, the excited wave is localized near the antenna with a standing wave character, and the dispersion relation of the helicon wave is not satisfied. After the jump, the excited wave propagates axially outwards and the dispersion relation of the helicon wave is confirmed both outside and inside the antenna regions.

Acknowledgment

We would like to thank Professor S-I Itoh for a critical reading of our manuscript.

References

[1] Boswell R W 1984 *Plasma Phys. Control. Fusion* **26** 1147
[2] Chen F F 1991 *Plasma Phys. Control. Fusion* **33** 339
[3] Komori A, Shoji T, Miyamoto K, Kawai J and Kawai Y 1991 *Phys. Fluids* B **3** 893
[4] Shoji T, Sakawa Y, Nakazawa S, Kadota K and Sato T 1993 *Plasma Sources Sci. Technol.* **2** 5
[5] Chen F F, Hsieh M J and Light M 1994 *Plasma Sources Sci. Technol.* **3** 49
[6] Yasaka Y and Hara Y 1994 *Japan. J. Appl. Phys.* **33** 5950
[7] Shoji T 1994 private communication
[8] Zhu P and Boswell R W 1991 *Phys. Fluids* B **3** 869
[9] Petržíka V 1993 *Research Report* IPPCZ-333, Institute of Plasma Physics, Czechoslovak Academy of Sciences
[10] Shinohara S, Asakura N, Naito M and Miyamoto K 1984 *J. Phys. Soc. Japan* **53** 1746
[11] Shinohara S, Naito O and Miyamoto K 1986 *Nucl. Fusion* **26** 1097
[12] Shinohara S, Naito O and Miyamoto K 1988 *J. Phys. Soc. Japan* **57** 665
[13] Amorim J, Maciel H S and Sudano J P 1991 *J. Vac. Sci. Technol.* B **9** 363